# SuperTIGER Abundances of Galactic Cosmic Rays for the Atomic Number ($Z$) Interval 30 to 56

**N.E. Walsh**$^{,*}$ **on behalf of the SuperTIGER Collaboration**
(a complete list of authors can be found at the end of the proceedings)

*Department of Physics and McDonnell Center for the Space Sciences, Washington University, St. Louis, MO 63130-4899, USA*

*E-mail:* newalsh@wustl.edu

SuperTIGER (Super Trans-Iron Galactic Element Recorder) is a long-duration-balloon instrument that completed its first Antarctic flight during the 2012-2013 austral summer, spending 55 days at an average float altitude of 125,000 feet. SuperTIGER measured the relative abundances of Galactic cosmic-ray (GCR) nuclei with high statistical precision and well resolved individual element peaks from $_{10}$Ne to $_{40}$Zr. SuperTIGER also made exploratory measurements of the relative abundances up to $_{56}$Ba. Although the statistics are low for elements heavier than $_{40}$Zr, we present preliminary relative abundance measurements of charges $Z = 41 - 56$ with individual element resolution. GCR measurements up to $_{40}$Zr support a source acceleration model where supernovae in OB associations preferentially accelerate refractory elements that are more readily embedded in interstellar dust grains than volatiles. In addition, injection into the GCR for both refractory and volatile elements appears to follow a charge dependence consistent with their grain sputtering cross sections. Our preliminary measurements of the $Z = 41 - 56$ range suggest the existence of an alternative GCR source or acceleration model for $Z > 40$ elements. We report progress in refining this interesting result.

*37$^{\text{th}}$ International Cosmic Ray Conference (ICRC 2021)*
*July 12th – 23rd, 2021*
*Online – Berlin, Germany*

---

$^*$Presenter

## 1. Introduction

Current observations point to OB associations as a major source of galactic cosmic ray (GCR) nuclei and to supernovae (SNe) as the main GCR accelerators. OB associations host the youngest and most massive stars which eject heavy nuclei through strong stellar winds and by exploding as supernovae (Higdon et al. 1998[1]). Subsequent supernova shock explosions sweep up this material, accelerating it to GCR energies(Wiedenbeck et al. 1999[2]). This acceleration is most efficient for high rigidity particles, and so refractory elements that are more likely to be embedded in dust grains with high mass to charge ratios are preferentially accelerated compared to volatile elements that are rarely embedded in grains (Lingenfelter 2019[3]).
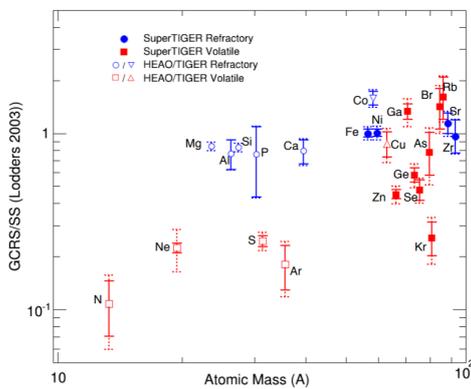


**(a)** GCRS abundances relative to Lodders 2003[4] so-solar system abundances. Figure from Murphy et al. 2016[5]. GCRS abundances from TIGER and HEAO-3-HNE are included (Rauch 2009[6]).
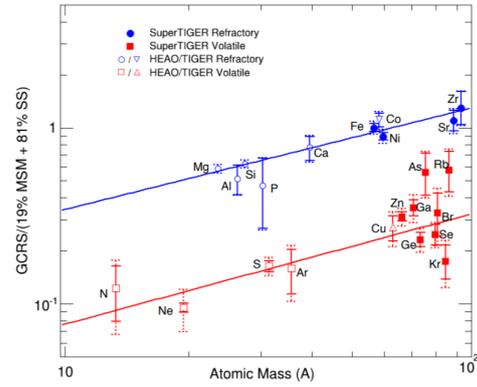
**(b)** GCRS abundances relative to a mix of 19% massive star material (Woosley and Heger 2007[7]) and 81% solar system material (Lodders 2003[4]). Figure from Murphy et al. 2016[5]. GCRS abundances from TIGER and HEAO are included where they were not replaced by those measured by SuperTIGER.

**Figure 1**

Plotting the GCR source abundances relative to solar system abundances shows that the refractory elements are more abundant in the GCR flux than volatiles, but only up to iron (Figure 1a). If, instead, we plot the GCR source abundances relative to a mix of solar system and massive star material, the refractory preferential acceleration model holds all the way up to zirconium (Figure 1b). As this material mixture is representative of the chemical makeup of OB associations (Binns et al. 2005[8], the fact that this mixture reveals the refractory enhancement model in the GCR abundance data is good evidence that GCR are being accelerated by supernovae from within OB associations. We aim to extend the SuperTIGER analysis up to barium, with atomic charge 56, to further test this theory of GCR origin and acceleration.

## 2. The SuperTIGER Instrument

The SuperTIGER instrument is optimized to measure UHGCR SuperTIGER is composed of two nearly identical, independently functioning detector stack modules, mounted side-by-side on

the balloon-payload gondola as in Figure 2a (Binns et al. 2014[9]). In each module (Figure 2b), a scintillating fiber hodoscope determines the trajectory of cosmic rays within the instrument. Three acrylic scintillators (S1, 2 and 3), one silica-aerogel Cherenkov detector (C0), and one acrylic Cherenkov detector (C1), with indices of refraction $n = 1.043$ (and 1.025 in one of four half-modules) and $n = 1.49$ respectively, are used in combination to determine the charge and energy of cosmic rays.
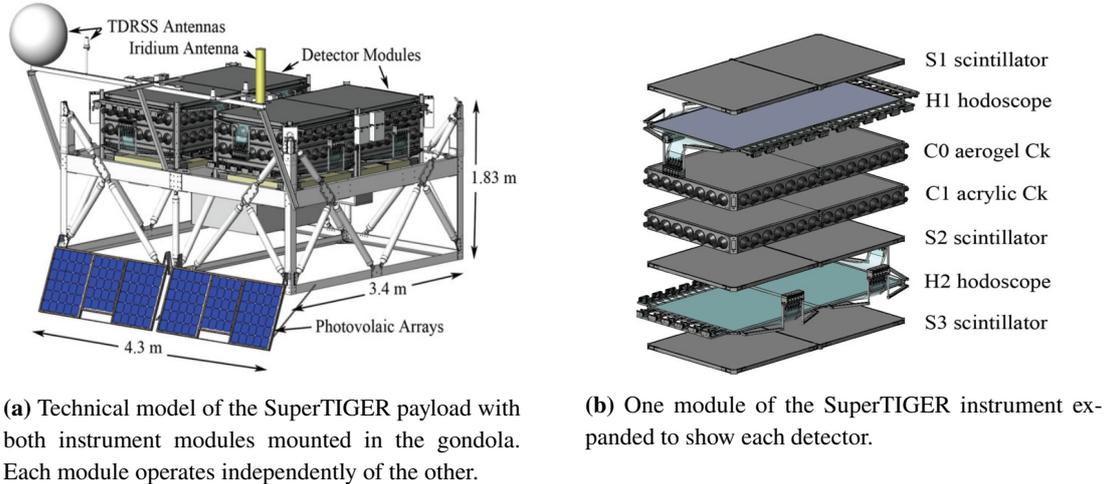


(a) Technical model of the SuperTIGER payload with both instrument modules mounted in the gondola. Each module operates independently of the other.

(b) One module of the SuperTIGER instrument expanded to show each detector.

**Figure 2**

The trajectory determined by the hodoscope is used to perform an angle correction on the summed photomultiplier tube signals obtained by the three scintillators and two Cherenkov detectors. The resulting corrected signal in each detector represents the light yield caused by a cosmic ray particle of a given charge that passes through. In this way, for every cosmic ray event, a charge estimate is made by each detector layer. These estimates are then used in combination during the analysis process (Section 3) to assign charge precisely. The turn on thresholds of the two Cherenkov detectors determine the measurement technique used to measure the charge of a cosmic ray with a given energy. The C1 detector responds to cosmic rays that deposit at least 320 MeV/nucleon, while the C0 detector turns on at 2.3 GeV/nucleon (or 3.3 GeV/nucelon for the $n = 1.025$ half-module). When a cosmic ray has energy greater than the C0 threshold, C1 and C0 can be used together in our "Above-C0" method. Otherwise, either S1 or S2 is used in combination with C1 in the "Below-C0" method.

## 3. Charge Assignment Method

When plotted together, the signals of these detectors form charge bands that are clearly visible up to nickel. In order to measure ultra heavy GCR (UHGCR), we must be able to assign charge to particles that are too scarce to form these dense charge bands.

As shown in Figure 3, we perform a cut on the C1 vs. C0 cross plot (right) that simulates the C0 energy threshold. We plot all the data to the left of this "Above-C0" cut on an S vs. C1 cross plot (left) and observe that this Below-C0 data is well resolved. In this way, we are able to assign charge with good resolution over most of the GCR energy range.
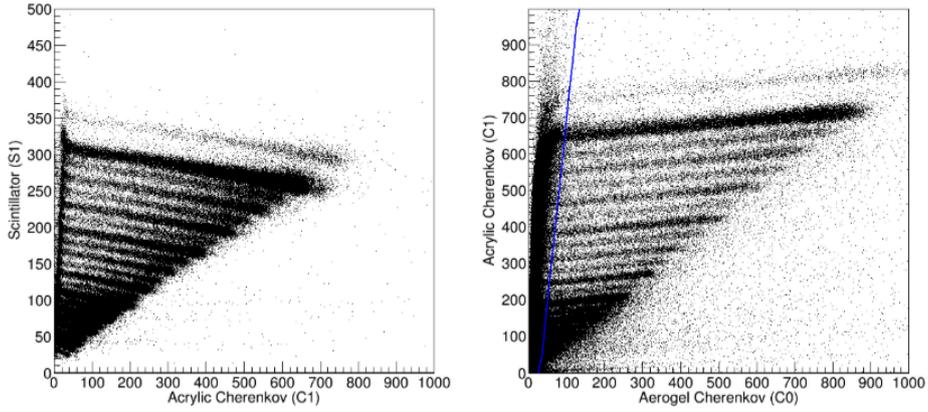
**Figure 3:** A single flight day's data is plotted in C1 vs. C0 space (right). The data to the left of the blue line is plotted in S1 vs. C1 space (left).

Fitting the charge bands determines the charge dependence of the band spacing (Figure 4). We extrapolate this dependence to the low statistics UH region above these bands. This is done differently for the Above-C0 and Below-C0 data sets.
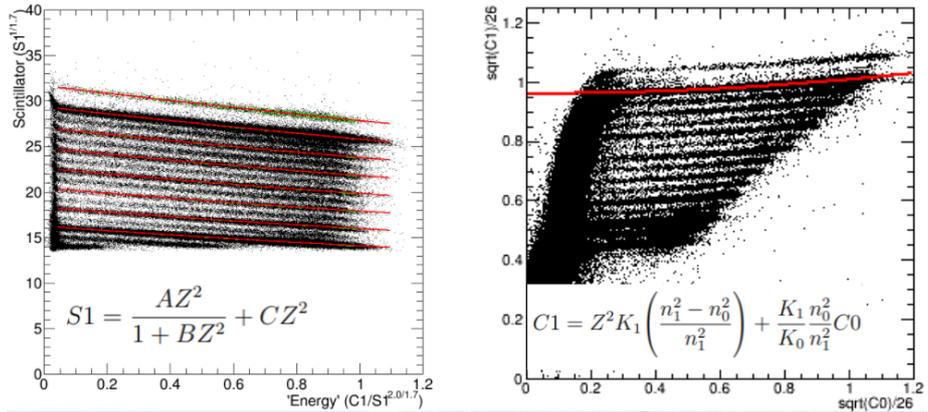


**Figure 4: Left:** Charge bands formed by one day of Below-C0 data within one angle bin. The even bands are fit by quadratics that are used to determine the charge-band spacing that is extrapolated to the UH region by the simplified Tarle saturation model displayed. **Right:** Charge bands formed by one day of Above-C0 data within one angle bin. The iron band is fit by a quadratic modification to the displayed linear equation, which is then used to extrapolate the charge-band spacing to the UH region.

For Above-C0, the band spacing is determined by the $Z^2$ factor in the y-intercept of the linear equation between shown in Figure 4(right). This linear equation describes the family of lines populated by cosmic ray events that yield two pure Cherenkov signals (C0 and C1), provided negligible energy loss occurs between the two Cherenkov materials. Because this equation represents the family of lines with separation $\propto Z^2$, it can be used to determine the charge of any particle given its two Cherenkov signals. While the linear relationship between C0 and C1 occurs for pure signals, in reality other small light contributions are present, such as scintillation from detector materials and additional Cherenkov from knock-on electrons. To account for residual effects, we fit the iron band with a quadradic, and use the resulting parameters to give charge to cosmic rays, given their

4

two Cherenkov signals.

For Below-C0, scintillator saturation effects complicate the charge dependence of the band spacing. In order to extract the charge dependence that allows us to determine the charge of a cosmic ray given the scintillator and acrylic cherenkov signals it produces, we fit each even-charge band ($16 \leq Z \leq 28$) with a quadratic, and, within each x-axis energy bin, we determine the scintillator signal value that corresponds to the charge of each of these bands. The simplified ($d\beta/dx = 0$) Tarle saturation model, shown in Figure 4(left), is then used to extrapolate the charge dependence of the scintillator response up into the UH region above the Below-C0 charge bands.

## 4. Obtaining GCRS Abundances

The charge histogram (Figure 5) resulting from plotting together the cosmic-ray events, with charges assigned by either the Above-C0 and Below-C0 methods described above, shows excellent individual element resolution up to zirconium. We also see well defined even-charge peaks up to barium. Due to very low statistics, the odd-charge peaks are particularly vulnerable to contamination from neighboring peaks. In addition, $Pd_{46}$ and $Cd_{48}$ appear spuriously low, possibly due to a gain matching issue currently under investigation. As such, the odd elements with $Z > 40$ are removed along with $Z = 46$ and 48 until we can account for these effects appropriately.

The measured abundances are extracted using a multi-peak Gaussian fit, where the sigma of each peak is allowed to vary linearly with charge. Because the resolution of odd-charge peaks will be poor due to contamination from the more abundant even charges, we use only the sigmas of the even charge-peaks with $16 \leq Z \leq 40$ to constrain the linearity of sigma over the measured charge range.
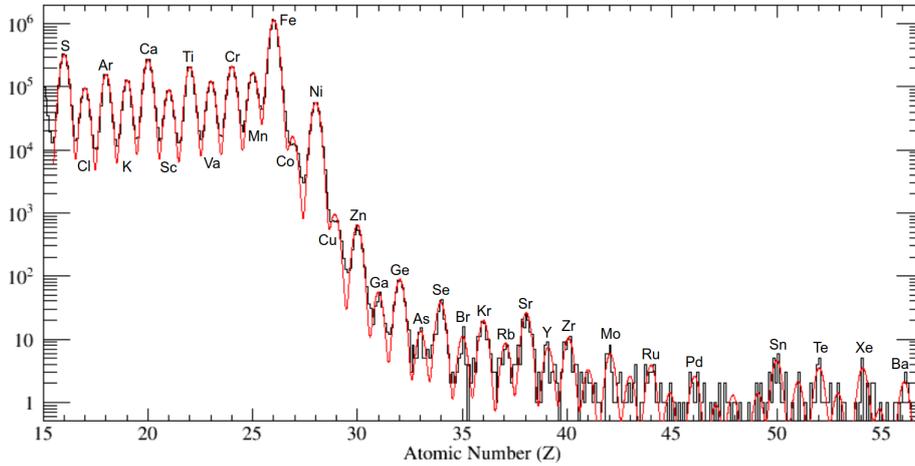


**Figure 5:** The entire measured SuperTIGER charge range ($16 \leq Z \leq 56$) fit by a multi-peak Gaussian function, with sigmas determined by a linear fit to the even-charge peak sigma values for peaks with $16 \leq 16 \leq 40$.

The extracted abundances are corrected for interactions and energy losses within the instrument, atmosphere and interstellar medium to obtain the abundances as they are at the top of the instrument (TOI), at the top of the atmosphere (TOA), and at the GCR source (GCRS), respectively. Comparing

the SuperTIGER TOA abundances to that of satellite results from HEAO3 and Ariel reveals good consistency all the way up to barium (Figure 6).
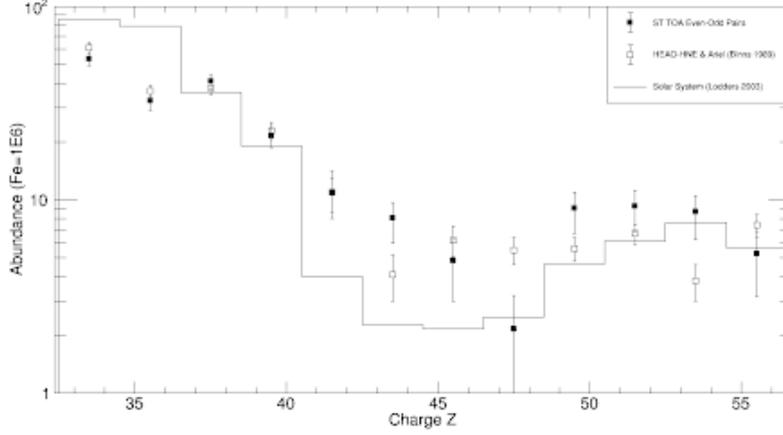


**Figure 6:** SuperTIGER TOA odd-even charge pair abundances for $33 \leq Z \leq 56$. Comparison to HEAO-3&Ariel odd-even charge pairs from Binns et al. 1989[10]. Solar system abundances from Lodders 2003[4] were also charge paired for comparison.

## 5.   Science Implications

To test the GCR origin and acceleration model, we plot the GCR source abundances relative to an OB association representative mix of 80% solar system and 20% massive star material (Figure 7). While the elements up zirconium show clear separation between refractory and volatile elements, it appears that the refractory preferential acceleration model does not hold for elements with charge greater than 40. It looks as if the volatile elements with $Z > 40$ are bumped up to the refractory enhancement line, instead of following their expected charge dependence line.

The breakdown of the refractory preferential acceleration model for elements with charge greater than 40 suggests that there might be a different production site or acceleration mechanism for these elements. One interesting observation is that the volatile elements in this range all have substantial contributions from r-process production (West and Heger 2013[11]). It is possible that there is an excess of r-process GCR for elements with $Z > 40$.

Binary neutron star mergers (BNSM) are known to produce vast amounts of r-process nuclei in a single event and some binary neutron star merger production models suggest that these events alone can account for the solar r-process abundances (Just et al. 2015[12]). It is interesting that the binary neutron star merger r-process production appears to fall off for $A = 90$ ($Z =\sim 40$), which is the point where the GCR source model appears to change. The rarity of BNSM events compared to that of SNe, as well as the unlikelihood for BNSM ejecta to be accelerated by nearby SNe, makes it difficult to explain how BNSM products could be enhanced in the GCR. Further work is required to probe this apparent change in model for GCR with $Z > 40$.
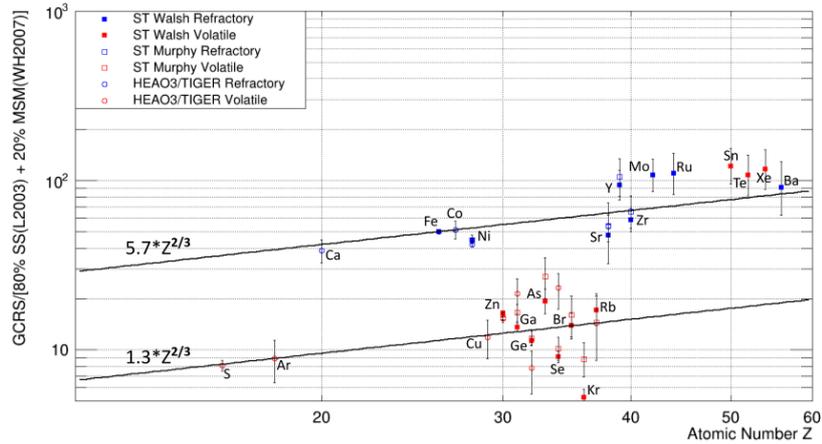
**Figure 7:** SuperTIGER GCRS abundances plotted relative to an OB association representative mix of 80% solar system material (Lodders 2003[4]) and 20% massive star material (Woosley and Heger 2007[7]). Odd elements with $Z > 40$ are removed along with $Z = 46$ and 48 due to poor statistics and large systematic uncertainties.

## References

[1] J. C. Higdon, R. E. Lingenfelter, and R. Ramaty. Cosmic-Ray Acceleration from Supernova Ejecta in Superbubbles. *The Astrophysical Journal*, 509:L33–L36, 1998.

[2] M. E. Wiedenbeck, W. R. Binns, E. R. Christian, A. C. Cummings, B. L. Dougherty, P. L. Hink, J. Klarmann, R. A. Leske, M. Lijowski, R. A. Mewaldt, E. C. Stone, M. R. Thayer, T. T. von Rosenvinge, and N. E. Yanasak. Constraints on the Time Delay Between Nucleosynthesis and Cosmic-Ray Acceleration From Observations of $^{59}$Ni and $^{59}$Co. *The Astrophysical Journal*, 523:L61–L64, 1999.

[3] Richard E. Lingenfelter. The Origin of Cosmic Rays: How Their Composition Defines Their Source and Sites and the Process of Their Mixing, Injection, and Acceleration. *The Astrophysical Journal Supplement Series*, 245:30, 2019.

[4] Katharina Lodders. Solar System Abundances and Condensation Temperatures of the Elements. *The Astrophysical Journal*, 519:1220–1247, 2003.

[5] R. P. Murphy, M. Sasaki, W. R. Binns, T. J. Brandt, T. Hams, M. H. Israel, A. W. Labrador, J. T. Link, R. A. Mewaldt, J. W. Mitchell, B. F. Rauch, K. Sakai, E. C. Stone, C. J. Waddington, N. E. Walsh, J. E. Ward, and M. E. Wiedenbeck. Galactic Cosmic Rays Origins and OB Associations: Evidence from SuperTIGER Observations of Elements $_{26}$Fe through $_{40}$Zr. *The Astrophysical Journal*, 831(2):148, 2016.

[6] B. F. Rauch, J. T. Link, K. Lodders, M. H. Israel, L. M. Barbier, W. R. Binns, E. R. Christian, J. R. Cummings, G. A. de Nolfo, S. Geier, R. A. Mewaldt, J. W. Mitchell, S. M. Schindler, L. M. Scott, E. C. Stone, R. E. Streitmatter, C. J. Waddington, and M. E. Wiedenbeck. Cosmic Ray

Origin in OB Associations and Preferential Acceleration of Refractory Elements: Evidence from Abundances of Elements $_{26}$Fe through $_{34}$Se. *The Astrophysical Journal*, 697(2):2083–2088, 2009.

[7] S. E. Woosley and A. Heger. Nucleosynthesis and Remnants in Massive Stars of Solar Metallicity. *Physics Reports*, 442:269–283, 2007.

[8] W. R. Binns, M. E. Wiedenbeck, M. Arnould, A. C. Cummings, J. S. George, S. Goriely, M. H. Israel, R. A. Leske, R. A. Mewaldt, G. Meynet, L. M. Scott, E. C. Stone, and T. T. von Rosenvinge. Cosmic-Ray Neon, Wolf-Rayet Stars, and the Superbubble Origin of Galactic Cosmic Rays. *The Astrophysical Journal*, 634:351–364, 2005.

[9] W. R. Binns, R. G. Bose, D. L. Braun, T. J. Brandt, W. M. Daniels, P. F. Dowkontt, S. P. Fitzsimmons, D. J. Hahne, T. Hams, M. H. Israel, J. Klemic, A. W. Labrador, J. T. Link, R. A. Mewaldt, J. W. Mitchell, P. Moore, R. P. Murphy, M. A. Olevitch, B. F. Rauch, K. Sakai, F. San Sebastian, M. Sasaki, G. E. Simburger, E. C. Stone, C. J. Waddington, J. E. Ward, and M. E. Wiedenbeck. The SuperTIGER Instrument: Measurement of Elemental Abundances of Ultra-Heavy Galactic Cosmic Rays. *The Astrophysical Journal*, 788:18, 2014.

[10] W. R. Binns, T. L. Garrard, P. S. Gibner, M. H. Israel, M. P. Kertzman, J. Klarmann, B. J. Newport, E. C. Stone, and C. J. Waddington. Abundances of Ultraheavy Elements in the Cosmic Radiation: Results from HEAO 3. *The Astrophysical Journal*, 346:997–1009, 1989.

[11] Christopher West and Alexander Heger. Metallicity-Dependent Galactic Isotopic Decomposition for Nucleosynthesis. *The Astrophysical Journal*, 744:75, 2013.

[12] O. Just, A. Bauswein, R. Ardevol Pulpillo, S. Goriely, and H.-T. Janka. Comprehensive Nucleosynthesis Analysis for Ejecta of Compact Binary Mergers. *Monthly Notices of the Royal Astronomical Society*, 448:541–567, 2015.

## Full Authors List: SuperTIGER Collaboration

Y. Akaike[1], W.R. Binns[2], R.G. Bose[2], T.J. Brandt[3], D. Braun[2], N. Cannady[4,5,6], P.F. Dowkontt[2], T. Hams[4,5,6], M.H. Israel[2], J.F. Krizmanic[4,5,6], A.W. Labrador[7], J.T. Link, R.A. Mewaldt[7], J.W. Mitchell[5] R.P. Murphy[2], G.A. de Nolfo[8], B.F. Rauch[2], K. Sakai[4,5,6], M. Sasaki[5,6,9], G. Simburger[2], E.C. Stone[7], T. Tatoli[8,10], N.E. Walsh[2], J.E. Ward[2], M.E. Wiedenbeck[11,7], W.V. Zober[2],

[1]Waseda Research Institute for Science and Engineering, Waseda University, Tokyo 162-0044, Japan

[2]Department of Physics and McDonnell Center for the Space Sciences, Washington University, St. Louis, MO 63130-4899, USA

[3]NASA Goddard Space Flight Center, Greenbelt, MD 20771, USA

[4]Center for Space Sciences and Technology, University of Maryland Baltimore County, Baltimore, MD 21250, USA

[5]Astroparticle Physics Laboratory, NASA/GSFC, Greenbelt, Maryland 20771, USA

[6]Center for Research and Exploration in Space Sciences and Technology, NASA/GSFC, Greenbelt, MD 20771, USA

[7]California Institute of Technology, Pasadena, CA 91125, USA

[8]Heliospheric Physics Laboratory, NASA/GSFC, Greenbelt, Maryland 20771, USA,

[9]Department of Astronomy, University of Maryland, College Park, Maryland 20742, USA,

[10]Department of Physics, Catholic University of America, Washington, DC 20064, USA

[11]Jet Propulsion Laboratory, Pasadena, CA 91109, USA